Molecular Cell, Volume *56*

Supplemental Information

Mechanism of Polyubiquitination by Human Anaphase-Promoting Complex: RING Repurposing for Ubiquitin Chain Assembly

Nicholas G. Brown, Edmond R. Watson, Florian Weissmann, Marc A. Jarvis, Ryan VanderLinden, Christy R. R. Grace, Jeremiah J. Frye, Renping Qiao, Prakash Dube, Georg Petzold, Shein Ei Cho, Omar Alsharif, Ju Bao, Iain F. Davidson, Jie J. Zheng, Amanda Nourse, Igor Kurinov, Jan-Michael Peters, Holger Stark, and Brenda A. Schulman

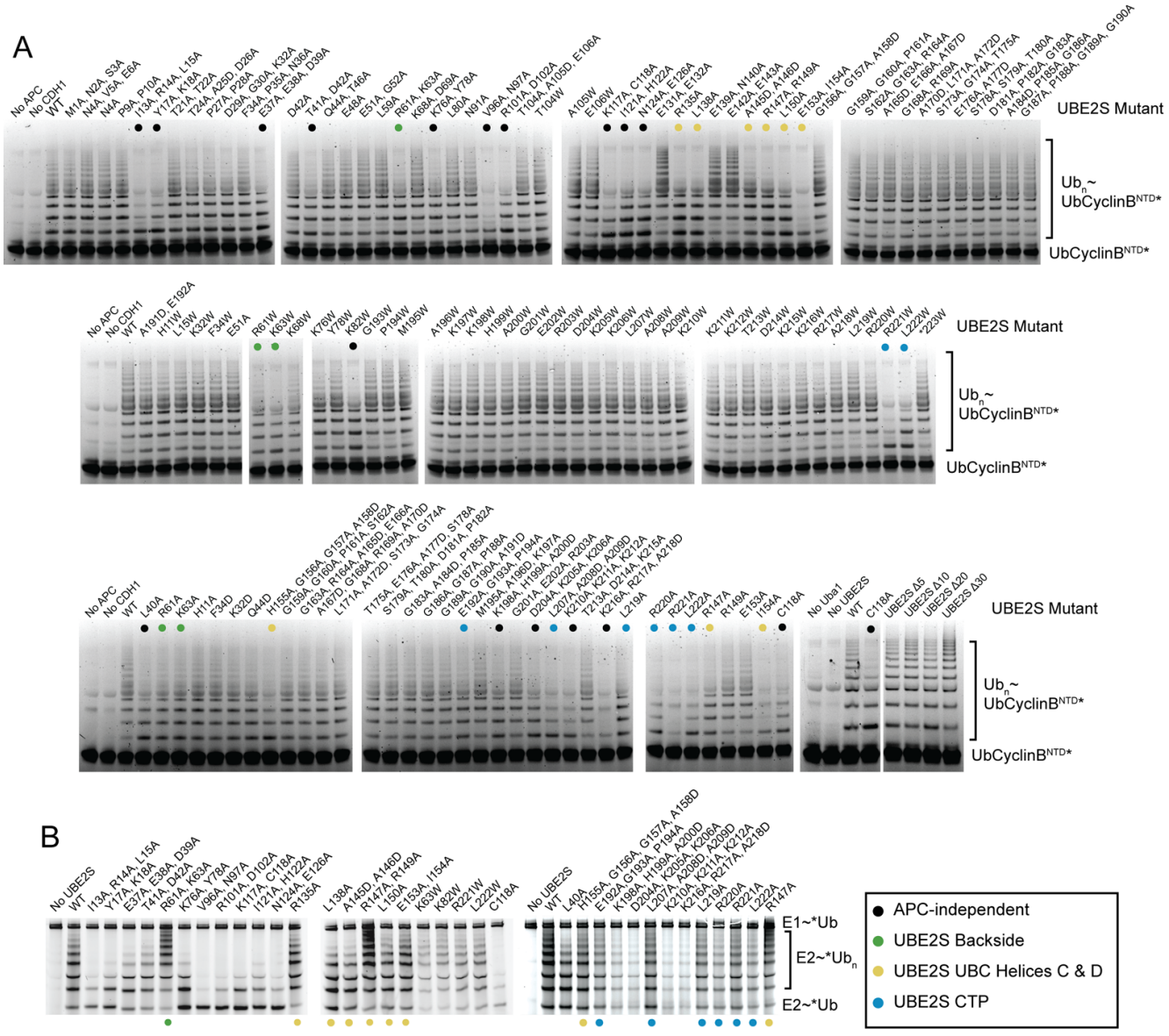
A
No APC
No CDH1
WT
M1A, N2A, S3A
N4A, V5A, E6A
N4A
P9A, P10A
I13A, R14A, L15A
Y17A, K18A
T21A, T22A
T24A, A25D, D26A
P27A, P28A
D29A, G30A, K32A
F34A, P35A, N36A
E37A, E38A, D39A
D42A
T41A, D42A
Q44A, T46A
E48A
E51A, G52A
L59A
R61A, K63A
K68A, D69A
K76A, Y78A
L80A
N91A
V96A, N97A
R101A, D102A
T104A, A105D, E106A
T104W
A105W
E106W
K117A, C118A
I121A, H122A
N124A, E126A
E131A, E132A
R135A
L138A
E139A, N140A
E142A, E143A
A145D, A146D
R147A, R149A
L150A
E153A, I154A
G156A, G157A, A158D
G159A, G160A, P161A
S162A, G163A, R164A
A165D, E166A, A167D
G168A, R169A
A170D, L171A, A172D
S173A, G174A, T175A
E176A, A177D
S178A, S179A, T180A
D181A, P182A, G183A
A184D, P185A, G186A
G187A, P186A, G189A, G190A
UBE2S Mutant
Ub$_n$~ UbCyclinB^{NTD*}
UbCyclinB^{NTD*}
No APC
No CDH1
WT
A191D, E192A
H11W
L15W
K32W
F34W
E51A
R61W
K63W
K68W
K76W
Y78W
K82W
G193W
P194W
M195W
A196W
K197W
K198W
H199W
A200W
G201W
E202W
R203W
D204W
K206W
L207W
A208W
A209W
K210W
K211W
K212W
T213W
D214W
K215W
K216W
R217W
A218W
L219W
R220W
R221W
L222W
*223W
UBE2S Mutant
Ub$_n$~ UbCyclinB^{NTD*}
UbCyclinB^{NTD*}
No APC
No CDH1
WT
L40A
R61A
K63A
H11A
F34D
K32D
Q44D
H155A, G156A, G157A, A158D
G159A, G160A, P161A, S162A
G163A, R164A, A165D, E166A
A167D, G168A, R169A, A170D
L171A, A172D, S173A, G174A
T175A, E176A, A177D, S178A
S179A, T180A, D181A, P182A
G183A, A184D, P185A
G186A, G187A, P188A
G189A, G190A, A191D
E192A, G193A, P194A
M195A, A196D, K197A
K198A, H199A, A200D
G201A, E202A, R203A
D204A, K205A, K206A
L207A, A208D, A209D
K210A, K211A, K212A
T213A, D214A, K215A
K216A, R217A, A218D
L219A
R220A
R221A
L222A
R147A
R149A
E153A
I154A
C118A
No Uba1
No UBE2S
WT
C118A
UBE2S Δ5
UBE2S Δ10
UBE2S Δ20
UBE2S Δ30
UBE2S Mutant
Ub$_n$~ UbCyclinB^{NTD*}
UbCyclinB^{NTD*}
B
No UBE2S
WT
I13A, R14A, L15A
Y17A, K18A
E37A, E38A, D39A
T41A, D42A
R61A, K63A
K76A, Y78A
V96A, N97A
R101A, D102A
K117A, C118A
I121A, H122A
N124A, E126A
R135A
L138A
A145D, A146D
R147A, R149A
L150A
E153A, I154A
K63W
K82W
R221W
L222W
C118A
No UBE2S
WT
L40A
H155A, G156A, G157A, A158D
E192A, G193A, P194A
K198A, H199A, A200D
D204A, K205A, K206A
L207A, A208D, A209D
K210A, K211A, K212A
K216A, R217A, A218D
L219A
R220A
R221A
L222A
R147A
E1~*Ub
E2~*Ub$_n$
E2~*Ub
APC-independent
UBE2S Backside
UBE2S UBC Helices C & D
UBE2S CTP

C

Data fitting for titrating UBE2S and variants in ubiquitination of Ub-CyclinB^{NTD*} by APC^{CDH1}

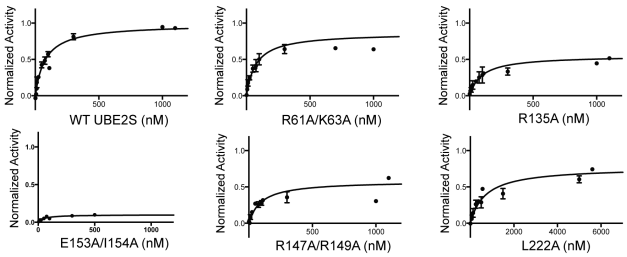

D

Data fitting for titrating UBE2S in di-Ub synthesis by APC variants

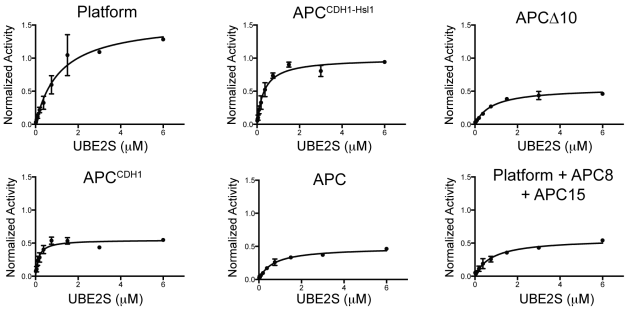

E

Data fitting for titrating Acceptor Ub in di-Ub synthesis by UBE2S and variants in the absence of APC

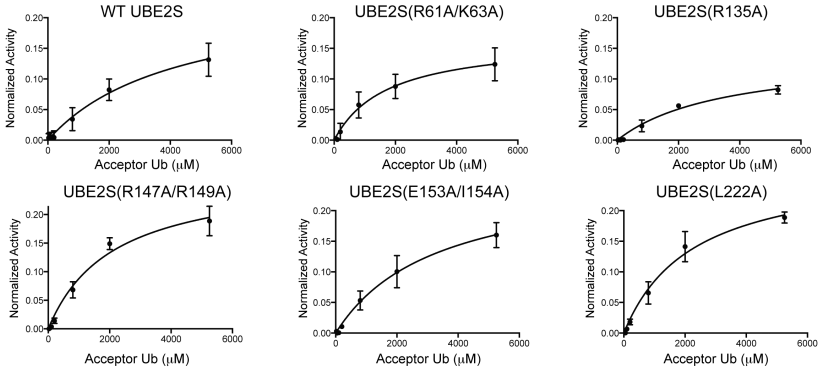

F

Data fitting for titrating Acceptor Ub in di-Ub synthesis by APC^{CDH1} with UBE2S and variants

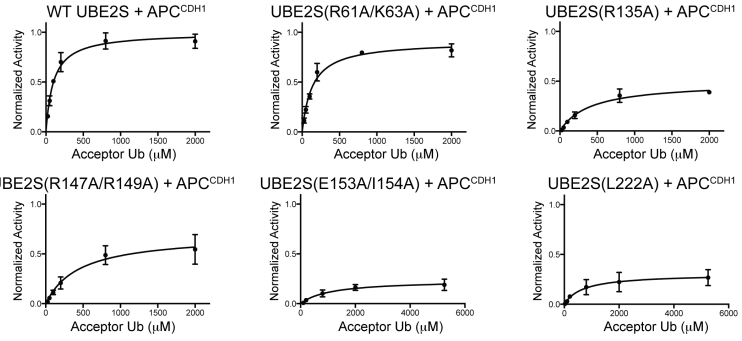

G

Data fitting for titrating UBE2S in ubiquitination of Ub-CyclinB^{NTD*} by APC^{CDH1} and APC11 RING mutants

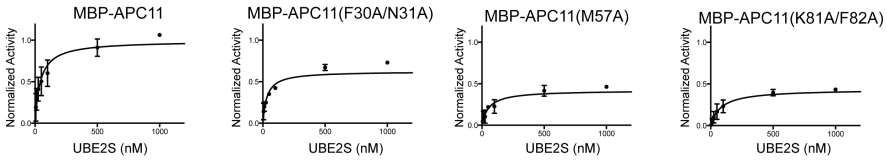

H

Data fitting for titrating Acceptor Ub in di-Ub synthesis by UBE2S and APC^{CDH1} and APC11 RING mutants

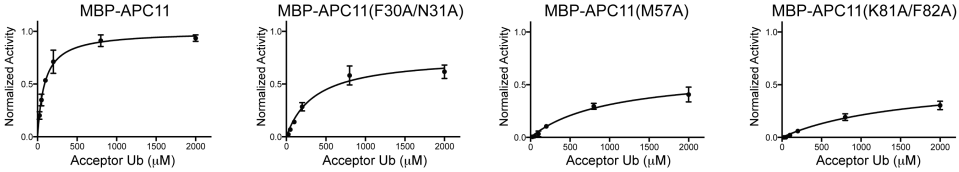

Figure S1. Representative fluorescence scans of raw SDS-PAGE data from UBE2S surface mutagenesis and fitting of kinetic data, related to Figure 1.

A, Data from 1st part of 2-part assay identifying UBE2S surfaces mediating APC-dependent ubiquitination. The need for an initiating E2 was bypassed by incorporating the priming Ub into a linear Ub-CyclinB^{NTD} fusion fluorescent substrate that is readily polyubiquitinated by APC^{CDH1}/UBE2S. Shown are representative fluorescence scans of raw SDS-PAGE data for Ub-CyclinB^{NTD}* ubiquitination by APC^{CDH1} and UBE2S (wild type and indicated mutant versions). Mutations causing decreased Ub-CyclinB^{NTD}* ubiquitination in presence of APC^{CDH1} are indicated with green, yellow and cyan dots, and structurally map to the backside of UBE2S' UBC domain, the C-terminal C and D helices of UBE2S' UBC domain, and the UBE2S C-terminal peptide (CTP), respectively. Black dots denote UBE2S mutants defective even in the absence of APC, identified in Fig. S1B. UBE2SΔ5, Δ10, Δ20, and Δ30 variants indicate that residues 181-186, 177-187, 167-187, and 160-190, respectively, were deleted from the UBE2S CTP.

B, 2nd part of 2-part assay identifying UBE2S surfaces mediating APC-dependent ubiquitination, filtering for APC-independent mutational defects by testing effects on UBE2S autoubiquitination. This reaction does not require APC, but as with APC-dependent ubiquitination, requires E1 charging and catalytic placement of the donor and acceptor Ub molecules. Shown are representative fluorescence scans of raw SDS-PAGE data monitoring autoubiquitination by fluorescent *Ub, with wild type UBE2S and the indicated mutant versions that were defective in the assay in Fig. S1A. Mutants specifically defective in APC-dependent ubiquitination shown above are indicated with green, yellow and cyan dots, based on their locations on the UBE2S structure.

C-H, Fitting of kinetic data. Error bars: SEM, n ≥ 3.
C, Titrations of UBE2S (wild type and indicated variants) in assays with fixed concentrations of APC^{CDH1} and Ub-CyclinB^{NTD}*.
D, Titrations of UBE2S (wild type and indicated variants) in di-Ub synthesis assays with fixed concentrations of APC variants and Ub*.
E, Titrations of acceptor Ub in di-Ub synthesis assays with fixed concentrations of UBE2S (wild type and indicated variants), without APC.
F, Titrations of acceptor Ub in di-Ub synthesis assays with fixed concentrations of APC^{CDH1} and UBE2S (wild type and indicated variants).
G, Titrations of UBE2S in assays monitoring ubiquitination of Ub-CyclinB^{NTD}*, with fixed concentrations of Ub-CyclinB^{NTD}* and APC^{CDH1} containing the indicated APC11 variants.
H, Titrations of acceptor Ub in di-Ub synthesis assays with fixed concentrations of APC^{CDH1} containing the indicated APC11 variants and UBE2S.

A

APC Subcomplex Name	APC Subunits	Figure
Platform Wild Type	APC1, APC4, APC5, APC2, APC11	2C, 2F, 2G
Platform MBP-11	APC1, APC4, APC5, APC2, His_6-MBP-APC11	2C
Platform MBP-11 ΔRING	APC1, APC4, APC5, APC2, His_6-MBP-APC11ΔRING	2C
APC 2/11	APC2 and APC11	2C, 2F, 3D
APC ΔAPC2 ΔAPC11	All APC Subunits except APC2 and APC11	2D
APC APC2 ΔCTD Δ11	All APC Subunits except APC11, and APC2 residues 1-548 only	2D
APC APC2 Δ4HB-CTD Δ11	All APC Subunits except APC11, and APC2 residues 1-445 only	2D
APC CFP-APC4ΔPropeller	All APC Subunits except APC4 residues 1-235 substituted with CFP	2D
Platform + APC8 + APC15	APC1, APC4, APC5, APC2, APC11, APC8, APC15	2G
APC ΔAPC10	All APC Subunits except APC10	2G
2/11 ΔRING	APC2 and APC11 ΔRING	3D
2 4HB-CTD/11	APC2 residues 446-822 and APC11	3D, 6C
2 4HB-CTD/MBP-11	APC2 residues 446-822 and His_6-MBP-APC11	3D
2 4HB-CTD/MBP-11ΔRING	APC2 residues 446-822 and His_6-MBP-APC11ΔRING	3D
APC MBP-APC11	All APC Subunits with His_6-MBP-APC11	4, 5A, 5B, 6A, 6B
2 4HB-CTD/11 ΔRING	APC2 residues 446-822 and APC11 ΔRING	6C
APC RING	APC11 residues 17-84	6D, 6E

B

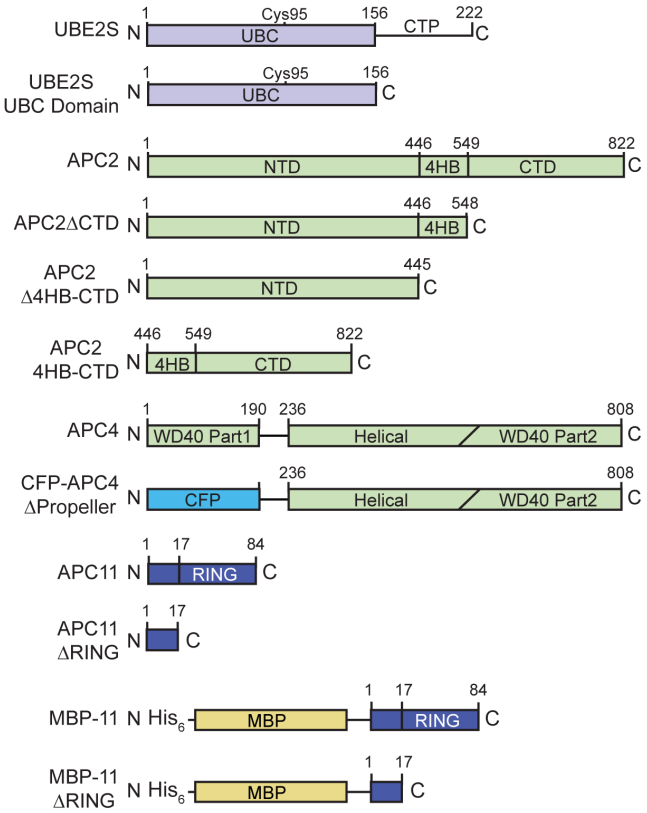

C

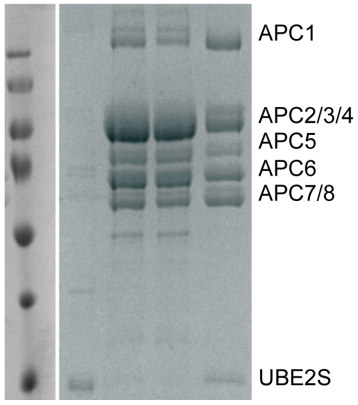

D

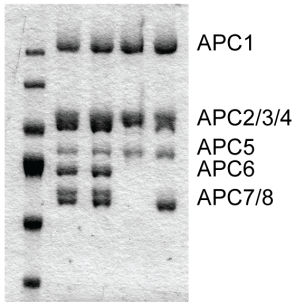

E

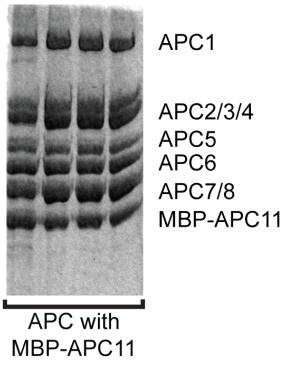

Figure S2. APC complexes and subcomplexes used in this study, related to Figure 2.

A, Table of APC complexes and subcomplexes, with names used in figures, their constituent APC subunits, and list of main figures in which they are used.

B, Schematic representation of primary structures of UBE2S, APC2, APC4, and various deletion mutants (not to scale). Domains of UBE2S: UBC – catalytic 'UBC' domain conserved among E2s; CTP – C-terminal peptide. Domains of APC2: NTD – N-terminal domain; 4HB – 4-helix bundle; CTD – C-terminal domain. Domains of APC4: WD40 – β-propeller; Helical – helical bundle domain. Domains of APC11: N-terminal domain followed by C-terminal RING domain; MBP – Maltose Binding Protein.

C, Affinity purification of recombinant APC bound to FLAG-tagged UBE2S used for EM. Coomassie-stained SDS-PAGE gel of the cryo-EM APC-UBE2S sample at different stages during the purification is shown. APC complexes used for scanning mutagenesis and immunoprecipitation analyses were purified based on affinity as shown, but those used in kinetic studies were further purified by ion exchange and gel filtration chromatography.

D, Coomassie-stained SDS-PAGE gel of purified APC subcomplexes used for kinetic studies in Fig. 2G.

E, Coomassie-stained SDS-PAGE gel of purified APC complexes containing His_6-MBP-APC11 RING mutants used for kinetic studies in Fig. 5B, 6A, 6B.

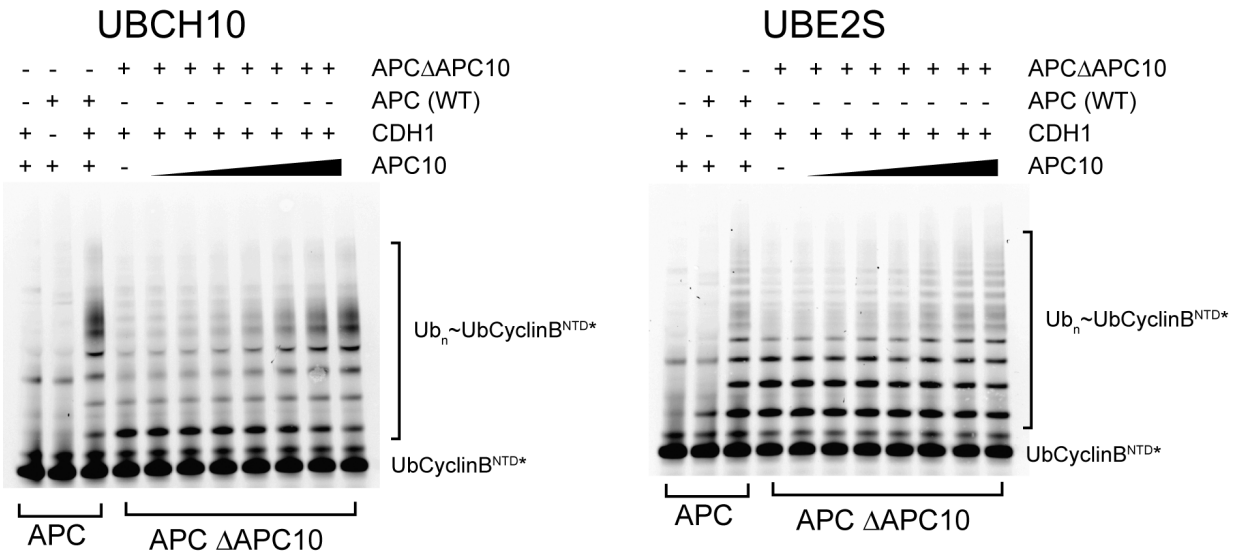

Figure S3. APC lacking APC10 is properly assembled, as addition of exogenous APC10 restores substrate-dependent ubiquitination activity, related to Figure 3. APC10 is required for processive APC^{CDH1}-dependent Ub-CyclinB^{NTD}* ubiquitination for both UBCH10 and UBE2S. Given a prior report that APC10 binds UBE2S (Sako et al., 2014), we also generated a version of APC lacking APC10, and validated its expected behavior toward Ub-CyclinB^{NTD}. Without APC10, which binds a substrate's D-box to enhance processivity of substrate ubiquitination, there was reduced generation of high molecular weight Ub conjugates on Ub-CyclinB^{NTD}*, but this was restored by adding bacterially expressed APC10 to reactions. Interestingly, however, deleting APC10 did not substantially influence either the K_m^{app} or V_{max}^{app} for UBE2S in di-Ub synthesis, which is independent of APC10's role in recruiting a substrate's D-box (Fig. 2G). Apparently, APC10 mediates its effects through means other than influencing the fundamental enzymatic function of forming Ub~Ub linkages.

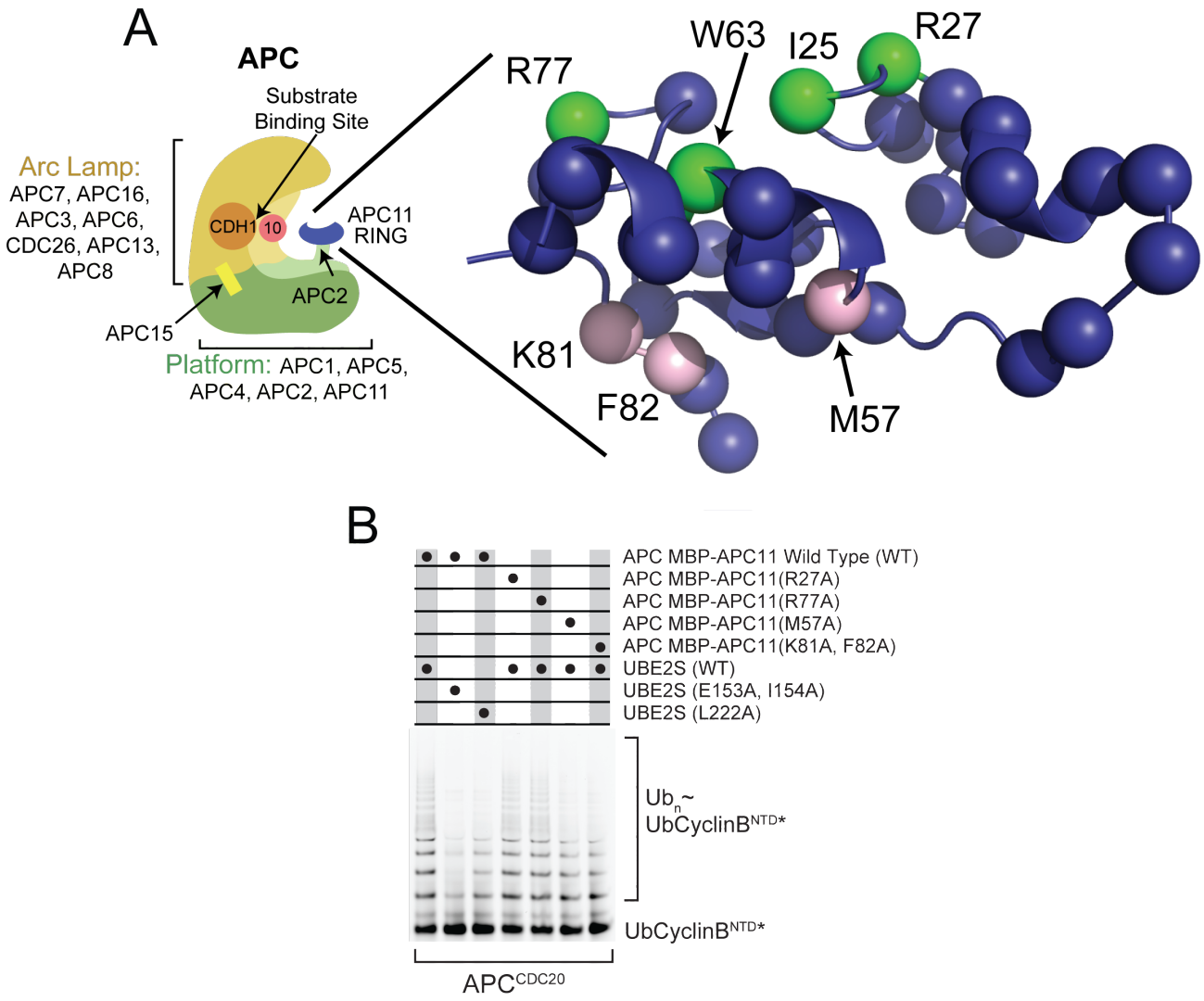

Figure S4. Alanine-scanning mutagenesis of APC11 RING domain within full APC complex, related to Figure 4.

A, Positions of Ala mutants are shown on the structure of the APC11 RING domain as spheres. APC complexes containing RING mutants were generated by coexpression of mutant versions of His_6-MBP-APC11 with all other APC subunits in insect cells. Canonical E2~Ub interacting residues for which mutations impaired ubiquitination by the Ub chain initiating E2s UBCH10 or UBCH5 are shown in green. Positions of mutations preferentially impairing ubiquitination by the Ub chain elongating E2, UBE2S, are shown in pink.

B, Mutations on UBE2S-specific RING surface, but not canonical E2~UB binding surface, impair Ub-CyclinB^{NTD*} polyubiquitination by APC^{CDC20}/UBE2S. Fluorescence scan of raw SDS-PAGE data.

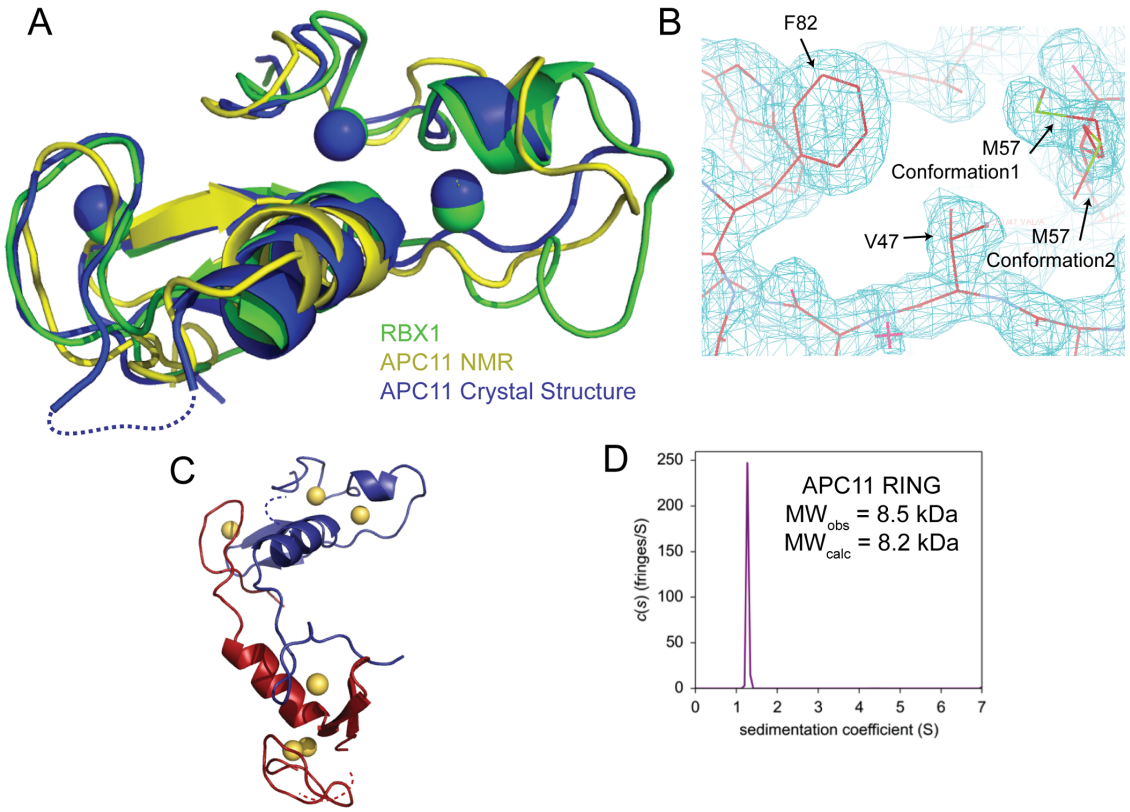

Figure S5. Structure determination of the human APC11 RING domain, related to Figure 5.

A, Crystal structure of APC11 RING domain in blue with zinc atoms as spheres, shown aligned with structure determined also by NMR (yellow) and the RING domain from RBX1 (green, from 1U6G.pdb, 0.94 RMSD (Goldenberg et al., 2004)). The crystal structure of the APC11 RING is a domain-swapped dimer. The domain swap occurs at the sequence Gln67-Gln68-Val69-Gln70-Gln71. For the figures of the APC11 RING domain structure, residues 21-68 are shown from one protomer, and 70-84 from the opposite protomer in the domain-swapped dimer to generate a single composite RING domain as shown here.

B, Representative electron density for the APC11 RING domain, shown over the surface involved in acceptor Ub recruitment in APC-UBE2S-mediated di-Ub synthesis. The side-chain of Met57 is modeled in two alternative conformations.

C, One domain swapped-dimer from the crystal structure of the APC11 RING domain. Two of four protomers in the asymmetric unit shown in blue and red, respectively, with zinc ions as yellow spheres.

D, Analytical ultracentrifugation data reveals the isolated APC11 RING domain protein samples used in the studies herein is predominantly monomeric in solution. The sedimentation velocity profiles (fringe displacement) were fitted to a continuous sedimentation coefficient distribution model c(s). The experiments were conducted in 25 mM Tris pH 7.6, 100 mM NaCl and 1 mM DTT buffer at 20 °C and at a rotor speed of 50,000 rpm. The measured molecular weight of 8.5 kDa corresponds well with the calculated mass of 8.2 kDa for a monomer.

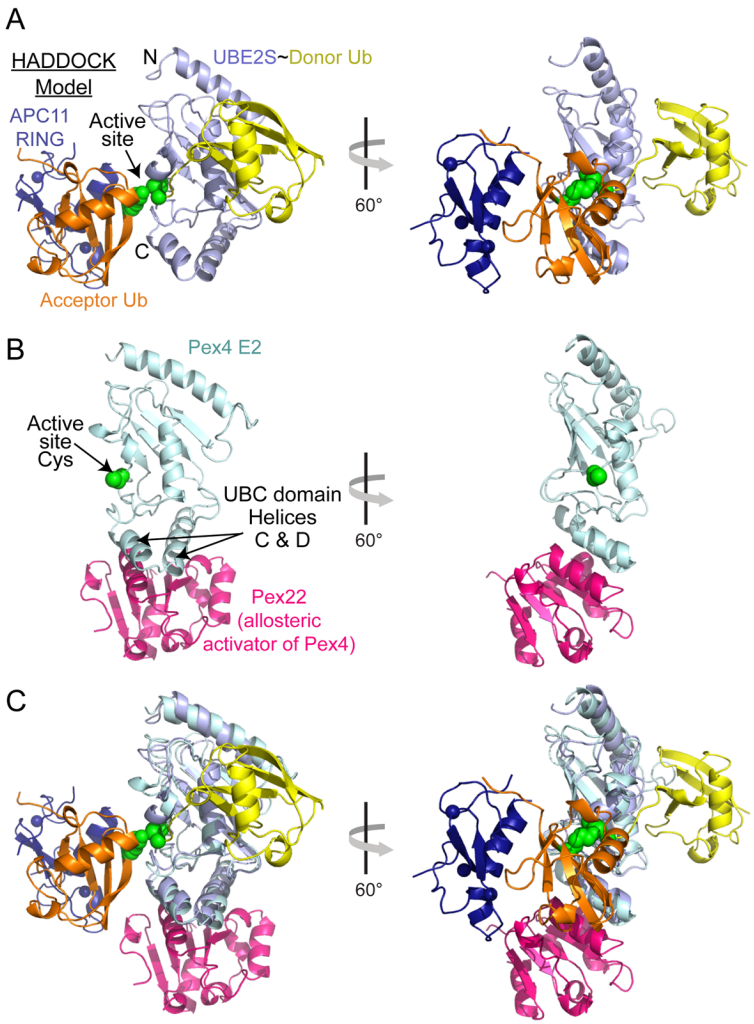

Figure S6. Structural modeling providing insights into distinctive RING-dependent APC activation of UBE2S-mediated Ub chain elongation, related to Figure 7.

A, Model of a ^{Donor}Ub~UBE2S-^{Acceptor}Ub-APC11 RING intermediate. Results of HADDOCK docking of APC11 RING (blue) with the acceptor Ub (orange) is modeled on the structure of the UBE2S UBC domain shown in slate (Sheng et al., 2012), according to (Wickliffe et al., 2011). The donor Ub (yellow) was modeled by aligning the structure of the UBE2S UBC domain and a structure of a ^{Donor}Ub~E2 complex (Plechanovova et al., 2012).

B, Structure of the *S. cerevisiae* E2 Pex4 (pale cyan) in complex with its activator, Pex22 (magenta), involved in a peroxisomal ubiquitination pathway (Williams et al., 2012). Notably, Pex22 interactions with Pex4 helices C and D allosterically activate Ub ligation through poorly defined mechanisms.

C, Compatibility and proximity of multiple modes of APC activation of Ub chain elongation with UBE2S. From APC, the APC11 RING helps recruit the acceptor Ub, and the APC2-APC4 region activates the UBE2S helix D. The interactions are compatible and spatially near each other as shown by superimposing the model in A for APC RING-dependent recruitment of the acceptor Ub to a UBE2S~Ub intermediate, and the UBC domain activation from the peroxisomal pathway in B.

Supplemental Experimental Procedures

Purification of proteins for enzyme assays, coimmunoprecipitation experiments, NMR, and crystallography

Recombinant APC and its subcomplexes were expressed in a baculovirus expression system similar to that described previously (Frye et al., 2013), although the only affinity tag was a twin-Strep tag at the C-terminus of APC4 similar to that used in recent structural studies (Chang et al., 2014). For all experiments other than EM and the experiments shown in Fig. 5A, APC, Platform, and other subcomplexes were purified with a 3-step scheme: Affinity purification with Strep-Tactin Sepharose (IBA Lifesciences) and elution with desthiobiotin, anion exchange, and size exclusion chromatography in a final buffer of 20 mM HEPES pH 8.0, 200 mM NaCl, 1 mM DTT. For the broad mutagenesis screen of RING domain mutants shown in Fig. 5A, APC complexes containing His_6-MBP-APC11 were purified by affinity chromatography based on the tag on APC4, with Strep-Tactin Sepharose, but APC incorporating RING mutants studied in Fig. 4, 5B, 6A, 6B, S1, and S4B were all purified using the 3-step scheme.

Wild type and mutant versions of UBE2S were expressed in BL21(DE3) Codon Plus (RIL) cells, from a modified pRSF-1b vector with a His_6-TEV protease site-FLAG-HRV13 3C protease site-fused to the N-terminus. For the Ala and Trp scanning mutagenesis described in Fig. 1D and S1, these were purified by nickel affinity chromatography, cleaved off the beads with HRV13 3C protease protease, and purified by cation exchange using gravity columns and bump elution with 20 mM TRIS pH 7.6, 400 mM NaCl, 1mM DTT. Concentrations of mutants were all normalized with this elution buffer prior to use, in order to ensure equal buffer and salt concentrations in assays. UBE2S and mutants used for kinetic and other follow-up enzyme assays (Fig. 1E, 2F-G, 3A-D, 4, 5A-B, 6A-B, 6F, S1C-H, S3 and S4B) were purified by nickel affinity chromatography, eluted, cleaved in solution by HRV13 3C protease, and further purified by cation exchange chromatography and size exclusion chromatography into a final buffer of 20 mM HEPES pH 8.0, 200 mM NaCl, 1 mM DTT. UBE2S and mutants used for FLAG immunoprecipitations in Fig. 2B, C, and D were purified by nickel affinity chromatography, eluted, and further purified by cation exchange using gravity columns and bump elution with 20 mM TRIS pH 7.6, 400 mM NaCl, 1mM DTT.

N-terminal 3xMYC-His_6-CDH1, 3xMYC-His_6-CDC20, UBCH10-His_6, and human E1 were purified as described previously (Frye et al., 2013; Uzunova et al., 2012). All other proteins were expressed in the BL21-CodonPlus(DE3)-RIL strain of *E. coli*, except the APC11 RING (residues 17-84) that was expressed in BL21-GOLD(DE3). APC11 RING domain for NMR was expressed as described previously for $EMI1^{ZT}$ in (Frye et al., 2013). Free APC10 and APC11 were expressed as a TEV protease cleavable N-terminal GST fusions, purified by glutathione-affinity chromatography and treated with TEV protease to cleave off the GST-tag. APC10 was further purified by cation exchange and size exclusion chromatography. APC11 was further purified with size exclusion chromatography. The $CyclinB^{NTD}$ (residues 1-95) and Ub-$CyclinB^{NTD}$ substrates were expressed as N-terminal GST fusions with a C-terminal Cys-His_6 tag and purified by nickel affinity chromatography, treated with TEV to remove tags, and polished with size exclusion chromatography. Untagged Ub was purified by an acetic acid precipitation step of unwanted bacterial proteins followed by cation exchange and size exclusion chromatography.

The Ub used as donor in assays in Figs. 1E, 2F-G, 3C-D, 4, 5A-B, 6A, S1C-D, S1G, S3, and S4B, and as acceptor in Figs. 3A-B, 6B, S1E-F, and S1H was purified largely as described previously (Pickart and Raasi, 2005). The fluorescent donor Ub (*Ub) for experiments in Figs. 3A-B, 6B, S1E-F, and S1H and the fluorescent acceptor Ub (Ub*) for experiments in Figs. 2F-G, 3D, and S1D were expressed as a N-terminal GST

fusion and purified by glutathione-affinity chromatography, TEV-mediated proteolytic cleavage of the GST-tag, and size exclusion chromatography. The fluorescent donor and acceptor ubiquitin contained a single cysteine at either position -1 or 77 (G75S:G76S:C77), respectively, for fluorescein-5-maleimide labeling described below. The Ub variants screened for ability to serve as acceptor Ub in Fig. 6F were expressed as Ub (1-74)-Ala-His_6 fusions and purified by nickel affinity chromatography, with buffer matching and removal of imidazole by desalting with PD-10 columns (GE Healthcare: Life Sciences) into 50 mM HEPES pH 7.0, 150 mM NaCl.

APC-UBE2S complex purification for cryo Electron Microscopy

APC was initially purified by incubation with Strep-Tactin Sepharose. After washing the Strep-Tactin resin, 5 µM His_6-TEV-FLAG-PreScission-UBE2S was incubated with resin-bound APC for 1 hour. The resin was washed with 50 mM HEPES pH 8.0, 150 mM NaCl, 2.5% glycerol, 0.05% Tween 20, and the APC-UBE2S complex was eluted with wash buffer supplemented with 2.5 mM desthiobiotin (Sigma). The eluate was then incubated with Anti-FLAG M2 affinity gel (Sigma) for 1 hour, washed with 50 mM HEPES pH 8.0, 150 mM NaCl, 2.5% glycerol, 0.05% Tween 20, and eluted with this wash buffer supplemented with 0.1 mg/ml FLAG peptide. The equivalent of 250 µg of APC-UBE2S was further processed through GraFix (Kastner et al., 2008).

Cryo Electron Microscopy

For cryo-EM, the buffer of GraFix-purified fractions was exchanged for 50 mM HEPES pH 8.0, 150 mM NaCl, 2 mM $MgCl_2$ by desalting (Zeba spin column, Pierce). Particles were adsorbed on carbon film for 1 minute and then mounted on an EM copper grid covered with a perforated carbon film. Specimens were blotted and vitrified (Vitrobot, FEI Company). Images were recorded at a magnification of 74,000x (2 Å/pixel) under cryogenic conditions in a C_s corrected Titan Krios (FEI Company) electron microscope on a Falcon II direct electron detector (FEI Company). The image dataset was corrected for the CTF (Sander et al., 2003) and particles were iteratively aligned applying resampling to polar coordinates (Sander et al., 2003) and multivariate statistical classification (van Heel, 1984). By computational sorting we found populations of APC particles with UBE2S bound in two distinct conformations and a population where UBE2S was lacking. Both APC/C-UBE2S 3D structures were calculated from ~20,000 particle images and a resolution of 13Å and 23Å were obtained (as judged by the FSC 0.143 criterion, calculated from two independently processed half datasets). Figures were generated using Chimera (Pettersen et al., 2004).

Enzyme Assays

The APC/C ubiquitination assays were performed as previously described (Frye et al., 2013), with some differences. The $CyclinB^{NTD}$ and Ub-$CyclinB^{NTD}$ substrates and fluorescent ubiquitins were labeled using fluorescein-5-maleimide (Pierce). Single cysteine proteins were first reduced with 20 mM DTT and desalted twice with Nap5 columns (GE Healthcare: Life Sciences) into 50 mM HEPES pH 7.0, 150 NaCl. The fluorescein-5-maleimide, dissolved in DMSO, was then added in 5-fold molar excess to the protein solution. The reaction was incubated at room temperature for ~2 hours. The reaction was then quenched with 10 mM DTT and subsequently desalted using a PD10 column into 50 mM HEPES pH 7.0, 150 NaCl, 10 mM DTT. Size exclusion chromatography was used to further remove the free fluorescent label using 20 mM HEPES pH 8.0, 200 mM NaCl, 1 mM DTT.

The assays were performed in the same buffer used for gel filtration of APC (20 mM HEPES pH 8.0, 200 mM NaCl, 1 mM DTT). Proteins were mixed on ice containing

APC, ubiquitination substrate (Ub, Ub*, *Ub, CyclinB^{NTD}* or Ub-CyclinB^{NTD}*) in 5 mM $MgCl_2$, 5mM ATP, 0.25 mg/mL BSA, with 1 μM CDH1 and 0.1 μM E1 and E2. The reaction mixtures were then equilibrated to room temperature before the reactions were initiated by adding 0.2 mM donor Ub. For all kinetic analyses, product bands were quantitated based on a fluorescein label on *Ub, Ub*, or Ub-CyclinB^{NTD}* using a Typhoon FLA 9500 PhosporImager. For APC-dependent Ub-CyclinB^{NTD}* reactions, APC-independent products were subtracted as background. For APC-independent reactions, products from a negative control reaction that did not contain the ^{Acceptor}Ub were subtracted as background.

Kinetic experiments to determine the apparent K_m (K_m^{app}) and apparent V_{max} (V_{max}^{app}) values were determined by fitting the initial velocities to the hyperbolic Michaelis-Menten, $v = V_{max}^{app}[X]/(K_m^{app} + [X])$, equation, where X is either the UBE2S or ^{Acceptor}Ub concentration, using GraphPad Prism 6 software. Single time points were taken under conditions that satisfy initial velocity regimes. In summary, a time course was monitored at both the minimum and maximum point of each titration to ensure a single time point could be taken where the substrate or UBE2S~Ub depletion are minimal and product formation remained linear. The activity for each quantitative assay was normalized to the V_{max}^{app} of wild-type UBE2S with either APC^{CDH1} or APC$^{CDH1\text{-}Hsl1}$ depending on the experiment described.

To determine the K_m^{app} and V_{max}^{app} values for UBE2S in assays monitoring Ub-CyclinB^{NTD}* ubiquitination or di-Ub synthesis using Ub* as the substrate, the concentrations were 10 nM or 30 nM APC variant, and 0.5 μM Ub-CyclinB^{NTD}* or 4 μM Ub*. Reactions were quenched after 10 min or 20 min, depending on the components. The assays monitoring Ub transfer to an acceptor Ub* were performed in similar conditions as assays for Ub-CyclinB^{NTD}* ubiquitination assays, except the acceptor substrate was Ub-fluorescein (G75S:G76S:C77). This C-terminal Cys is fluorescently labeled and prevents the Ub-fluorescein from conjugating to either the E1 or E2. For the assays monitoring ubiquitination of Ub-CyclinB^{NTD}*, the data were normalized to the V_{max}^{app} of wild type UBE2S-APC^{CDH1}. For the assays monitoring Ub transfer to Ub*, the data were normalized to the V_{max}^{app} of wild type UBE2S-APC$^{CDH1\text{-}Hsl1}$.

Qualitative assays probing the function of UBE2S were performed as described above except with concentrations of 14 nM APC, 0.25 μM UBE2S, 0.5 μM Ub-CyclinB^{NTD}* were used (Fig. 1D and S1A). These reactions were quenched at 10 min. The UBE2S autoubiquitination assays (Fig. 1D and S1B) were carried out similarly except (1) the only Ub source was fluorescein-labeled wild type *Ub used at 4 μM concentration; (2) APC^{CDH1} and Ub-CyclinB^{NTD}* were absent; and (3) the reactions were quenched after 60 min.

Qualitative assays probing the function of His_6-MBP-APC11 RING domain in the context of APC (Fig. 5A) were performed as described above except concentrations of 50 nM APC, 1 μM CDH1, 0.2 μM UBCH5B, UBCH10 or UBE2S, 0.2 μM CyclinB^{NTD} or Ub-CyclinB^{NTD}* were used. These reactions were quenched at 15 min. Qualitative assays in Figs. 4, 5B, and S3 were performed similarly, except the APC concentration is 30 nM APC and in Fig S4B, 0.6 μM CDC20 was used instead of CDH1.

To determine the K_m^{app} and V_{max}^{app} values for the acceptor Ub, 20 μM of the fluorescein-labeled wild-type *Ub was first loaded onto 10 μM E1 in the presence of 5 mM MgCl2 and 5 mM ATP for 10 min at room temperature. Formation of the E1~*Ub intermediate was quenched with 25 mM EDTA and two passes over desalting columns (Zeba spin column, Pierce) to remove and/or chelate the MgATP to prevent reloading of the E1. The E1~*Ub was then diluted into a second independent mixture (final concentration 2 μM E1~*Ub) that contained unlabeled Ub, BSA, 0.2 μM UBE2S and 0.1 μM APC^{CDH1}, and ubiquitination reactions were then carried out for 3 min. The data were normalized to the V_{max}^{app} of wild type UBE2S-APC^{CDH1}.

For qualitative assays probing the function of the acceptor Ub mutants (Fig. 6F), the E1 charging reaction was started with addition of E1, Ub and MgATP. Formation of the E1~Ub intermediate was quenched by adding EDTA and subsequent desalting. The reaction was then added to a mixture containing UBE2S and Ub or UBE2S, APC^{CDH1}, and Ub. The Ub (1-74)-Ala-His_6 fusion variants were screened in the APC^{CDH1}-independent and APC^{CDH1}-dependent assays at concentrations similar to the apparent K_m^{app} values for wild type acceptor Ub as follows: 0.1 μM APC^{CDH1}, 2 μM UBE2S, and 0.1 mM Ub for 5 min in the APC^{CDH1}-dependent assay and 20 μM UBE2S and 1 mM Ub for 15 min in the APC^{CDH1}-independent assay. The UBE2S and Ub concentrations used in APC-dependent and APC-independent assays differ to compensate for the different K_m^{app} and V_{max}^{app} values in the presence or absence of APC^{CDH1}.

BPA-UBE2S Protein Expression and Purification

Amber codons and deletion of CTP "LRRL" residues of UBE2S mutants were introduced into pGEX modified with GST-TEV-FLAG-PreScission. These various amber codon-containing UBE2S constructs were co-transformed into BL21(DE3) with pEVOL-*pBpF*, a plasmid that encodes aaRS for *p*-Benzoyl-L-Phenylalanine (BPA) and modified tRNA that repurposes the TAG codon for ribosomal incorporation of BPA (Addgene plasmid 31190) (Young et al., 2010). Proteins were expressed overnight at 23° in auto-induction media and induced simultaneously with 0.02% Arabinose (Sigma), 0.6 mM IPTG, and 0.2 mM BPA dissolved immediately prior to use at 50 mM in 0.7 M NaOH. BPA-UBE2S proteins were purified by glutathione-affinity and cation exchange chromatography. Incorporation of BPA was verified by Intact Mass Spectrometry for the BPA-UBE2S variants (Hartwell Center, St. Jude Proteomics/Mass Spectrometry Facility). *p*-Benzoyl-L-Phenylalanine (BPA) was purchased from Bachem.

Photocrosslinking BPA-UBE2S with APC

Photocrosslinking experiments were performed on ice by mixing BPA-UBE2S with APC-His_6-MBP-APC11 and 3xMYC-His_6-CDH1 at 1 μM. Following a 60-minute exposure to 365nm UV light (Bulb ID: 34-0009-01) proteins were separated by 15% (FLAG-UBE2S blot) or 8% (APC subunit blots) SDS-PAGE. The following commercial antibodies were used for detection in crosslinking studies by western blotting using standard methods: APC1 (SC-20983, SCBT), APC2 (12301, Cell Signaling Technology), APC4 (SC-21414, SCBT), APC11 (14090, Cell Signaling Technology), Strep-Tag II (Ab76949, Abcam), FLAG (F1804, Sigma-Aldrich), and c-MYC (SC-40, SCBT). Polyclonal APC5 antibodies were generated at Gramsch Laboratories against a synthetic peptide (ELTSRDEGERKMEKEEL).

X-Ray Crystallography

APC 11 RING domain (residues 17-84) was purified in 25 mM TRIS pH 7.6, 100 mM NaCl, 1 mM DTT. Crystals were grown with the hanging drop vapor diffusion method in 16% PEG 3350, 0.2 M $NaNO_3$, 0.1 M BIS-TRIS Propane pH 6.5 and set at room temperature with 30 mg/mL APC11 RING domain. The mother liquor including 40% PEG 3350 was used as a cryoprotectant. The data were collected at NECAT ID-24C at the Zn peak energy. The data were integrated and scaled using the NECAT RAPD software (https://rapd.nec.aps.anl.gov/rapd). The initial phasing electron density was obtained with zinc SAD using SHELX (Sheldrick, 2008). Model construction and refinement were done in Coot (Emsley and Cowtan, 2004; Emsley et al., 2010) and Phenix (Adams et al., 2010).

NMR Spectroscopy

NMR samples were purified in 20 mM Hepes pH 7.0, 100 mM NaCl, 10 mM DTT dissolved in 90% H_2O/10% D_2O buffer. All the titration data were collected as 2D [^{15}N, ^{1}H] TROSY spectra at 298K with a Bruker 800 MHz spectrometer equipped with a ^{1}H and ^{13}C detector, TCI triple resonance cryogenic probe on ^{15}N-labeled samples. The assays monitoring chemical shift perturbations upon adding $APC2^{4HB\text{-}CTD}$ /APC11±RING to ^{15}N-labeled Ub were performed at concentrations of 0.24 mM and 0.1 mM, respectively. An APC11 RING titration ranging from 0.1 - 1.3 mM was added to 0.2 mM ^{15}N-labeled Ub. An Ub titration ranging from 0.2 - 3 mM was added to 0.1 mM ^{15}N-labeled APC11 RING. RING domain assignment experiments were carried out on ^{15}N, ^{13}C labeled APC11 RING at 500 µM concentration. APC11 RING domain backbone resonance 3D NMR experiments were measured on a Bruker 600 MHz spectrometer equipped with a ^{1}H and ^{13}C detect, TCI triple resonance cryogenic probe using standard Bruker pulse programs. ^{1}H, ^{13}C, and ^{15}N backbone resonances were assigned using standard triple resonance experiments, such as HNCACB, CBCA(CO)NH, HNCO and HN(CA)CO. Side chain assignments were carried out using ^{15}N-resolved TOCSY, ^{13}C-resolved H(C)CH TOCSY and (H)CCH TOCSY experiments. Aromatic side chains were assigned using the 13C-resolved aromatic NOESY spectra along with the TOCSY. All the ^{1}H chemical shifts were referenced with respect to DSS measured in the same buffer, while the ^{13}C and ^{15}N chemical shifts were referenced indirectly with respect to the DSS shift. All of the spectra were processed using TopSpin software and analyzed using the computer-aided resonance software, CARA (Keller, 2004). Ubiquitin assignments were taken from BMRB entry 15410 (Wong et al., 2008). The chemical shift perturbations were calculated using, $CSP(ppm) = [(\Delta\delta H)^2 + (1/2)(\Delta\delta N)^2]^{0.5}$, where $\Delta\delta H$ and $\Delta\delta N$ represents the chemical shift difference between the free and complex for ^{1}H and ^{15}N resonances respectively.

Structures were determined using a combination of manually assigned NOEs and automatic NOE assignment using the program CYANA (Guntert et al., 1997). Approximately 872 meaningful distance restraints, 32 angle restraints derived from CA, CB shifts using program TALOS+(Shen et al., 2009), 12 zinc ion distances and 18 hydrogen bond restraints based on exchange cross peaks with water in the ^{15}N-NOESY spectrum, were used in the structure calculation of APC11 RING. Seven iterations of refinement of 100 structures per cycle were completed, after proper distance calibrations. After the initial fold of the protein was determined, a CYANA amino acid library using a modified zinc-ligated cysteine residue was used to incorporate the three zinc ions into the structures. Parameters used in the structure calculation are given in Table 2.

Analytical Ultracentrifugation

Sedimentation velocity experiments were conducted in a ProteomeLab XL-I analytical ultracentrifuge (Beckman Coulter, Indianapolis, IN) following standard protocols unless mentioned otherwise (Zhao et al., 2013a). The sample in a buffer containing 25 mM Tris pH 7.6, 100 mM NaCl, and 1 mM DTT was loaded into a cell assembly comprised of a double sector charcoal-filled centerpiece with a 12 mm path length and sapphire windows. The density and viscosity of the ultracentrifugation buffer at 20 °C were measured with a DMA 5000M density meter and an AMVn viscometer (both Anton Paar, Graz, Austria) respectively. The cell assembly, containing identical sample and reference buffer volumes of 400 µL, was placed in a rotor and temperature equilibrated at 20 °C at rest for 2 hours before it was accelerated from 0 to 50,000 rpm. Rayleigh interference optical data were collected at 1-minute intervals for 12 hours. The velocity data were modeled with diffusion-deconvoluted sedimentation coefficient distributions c(s) in SEDFIT (https://sedfitsedphat.nibib.nih.gov/software/default.aspx), using algebraic noise decomposition and with signal-average frictional ratio and meniscus position refined with

non-linear regression. The s-value was corrected for time, temperature and radial position and finite acceleration of the rotor was accounted for in the evaluation of Lamm equation solutions (Ghirlando et al., 2014; Zhao et al., 2013b). Maximum entropy regularization was applied at a confidence level of P-0.68.

Computational modeling APC11 RING-^{Acceptor}Ub interactions

We used Haddock 2.1 (de Vries et al., 2007; Dominguez et al., 2003) for constructing the RING-^{Acceptor}Ub complex. The HADDOCK run produced an ensemble of 200 structures, which were clustered by applying backbone root-mean-square deviation (rmsd) cut-off of 7.5 angstrom after two-step HADDOCK simulations. To model the RING-^{Acceptor}Ub complex, the crystal structure of the APC11 RING domain was docked to a single Ub molecule. The binding interface of the RING domain and acceptor Ub was defined from NMR chemical shift perturbation data by mutual titrations of the RING domain and ubiquitin. Two loops of the acceptor Ub, residues 8-10 and 72-76, were set as flexible residues in explicit solvent refinement stage, to allow the system to fully explore more favorable conformations of these regions while maintaining the overall complex architecture. Interactions of side chains with three zinc ions were kept during simulations by adding additional unambiguous distance restraints. The simulation generated 2 clusters. The cluster 1 contains 87% of all modeled structures with better average binding affinity within the top ranked four structures as shown below:

The calculated binding free energies of top ranked models in the two HADDOCK clusters.

	Number of Structures[b]	**E_{tot}[c] (k_{cal}/mol)**	**E_{vdw}[d] (k_{cal}/mol)**	**E_{elec}[e] (k_{cal}/mol)**
Cluster 1 (top 4)[a]	164	-3.37 +/- 0.22	-0.83 +/- 0.30	-2.54 +/- 0.33
Cluster 2 (top 4)	26	-0.63 +/- 0.63	-0.50 +/- 0.49	-0.13 +/- 0.67

[a] The top four models with best binding free energies from each cluster were used to determine the average binding free energies and standard deviations .

[b] Indicates that the number of structures in each cluster which share similar conformations with backbone rmsds within 7.5 angstroms.

[c] E_{tot} indicates the total binding free energy.

[d] E_{vdw} indicates the average van der waals interaction energy.

[e] E_{elec} indicates the average electrostatic interaction energy.

SUPPLEMENTAL REFERENCES

Adams, P.D., Afonine, P.V., Bunkoczi, G., Chen, V.B., Davis, I.W., Echols, N., Headd, J.J., Hung, L.W., Kapral, G.J., Grosse-Kunstleve, R.W.*, et al.* (2010). PHENIX: a comprehensive Python-based system for macromolecular structure solution. Acta crystallographica *66*, 213-221.

Chang, L., Zhang, Z., Yang, J., McLaughlin, S.H., and Barford, D. (2014). Molecular architecture and mechanism of the anaphase-promoting complex. Nature.

de Vries, S.J., van Dijk, A.D., Krzeminski, M., van Dijk, M., Thureau, A., Hsu, V., Wassenaar, T., and Bonvin, A.M. (2007). HADDOCK versus HADDOCK: new features and performance of HADDOCK2.0 on the CAPRI targets. Proteins *69*, 726-733.

Dominguez, C., Boelens, R., and Bonvin, A.M. (2003). HADDOCK: a protein-protein docking approach based on biochemical or biophysical information. Journal of the American Chemical Society *125*, 1731-1737.

Emsley, P., and Cowtan, K. (2004). Coot: model-building tools for molecular graphics. Acta crystallographica *60*, 2126-2132.

Emsley, P., Lohkamp, B., Scott, W.G., and Cowtan, K. (2010). Features and development of Coot. Acta crystallographica *66*, 486-501.

Frye, J.J., Brown, N.G., Petzold, G., Watson, E.R., Grace, C.R., Nourse, A., Jarvis, M.A., Kriwacki, R.W., Peters, J.M., Stark, H.*, et al.* (2013). Electron microscopy structure of human APC/C(CDH1)-EMI1 reveals multimodal mechanism of E3 ligase shutdown. Nature structural & molecular biology *20*, 827-835.

Ghirlando, R., Zhao, H., Balbo, A., Piszczek, G., Curth, U., Brautigam, C.A., and Schuck, P. (2014). Measurement of the temperature of the resting rotor in analytical ultracentrifugation. Anal Biochem *458*, 37-39.

Goldenberg, S.J., Cascio, T.C., Shumway, S.D., Garbutt, K.C., Liu, J., Xiong, Y., and Zheng, N. (2004). Structure of the Cand1-Cul1-Roc1 complex reveals regulatory mechanisms for the assembly of the multisubunit cullin-dependent ubiquitin ligases. Cell *119*, 517-528.

Guntert, P., Mumenthaler, C., and Wuthrich, K. (1997). Torsion angle dynamics for NMR structure calculation with the new program DYANA. Journal of molecular biology *273*, 283-298.

Kastner, B., Fischer, N., Golas, M.M., Sander, B., Dube, P., Boehringer, D., Hartmuth, K., Deckert, J., Hauer, F., Wolf, E.*, et al.* (2008). GraFix: sample preparation for single-particle electron cryomicroscopy. Nat Methods *5*, 53-55.

Keller, R.L.J. (2004). Computer Aided Resonance Assignment Tutorial. http://cara.nmr-software.org/downloads/3-85600-112-3.pdf.

Pettersen, E.F., Goddard, T.D., Huang, C.C., Couch, G.S., Greenblatt, D.M., Meng, E.C., and Ferrin, T.E. (2004). UCSF Chimera--a visualization system for exploratory research and analysis. J Comput Chem *25*, 1605-1612.

Pickart, C.M., and Raasi, S. (2005). Controlled synthesis of polyubiquitin chains. Methods in enzymology *399*, 21-36.

Plechanovova, A., Jaffray, E.G., Tatham, M.H., Naismith, J.H., and Hay, R.T. (2012). Structure of a RING E3 ligase and ubiquitin-loaded E2 primed for catalysis. Nature *489*, 115-120.

Sako, K., Suzuki, K., Isoda, M., Yoshikai, S., Senoo, C., Nakajo, N., Ohe, M., and Sagata, N. (2014). Emi2 mediates meiotic MII arrest by competitively inhibiting the binding of Ube2S to the APC/C. Nature communications *5*, 3667.

Sander, B., Golas, M.M., and Stark, H. (2003). Corrim-based alignment for improved speed in single-particle image processing. Journal of structural biology *143*, 219-228.

Sheldrick, G.M. (2008). A short history of SHELX. Acta Crystallogr A *64*, 112-122.

Shen, Y., Delaglio, F., Cornilescu, G., and Bax, A. (2009). TALOS+: a hybrid method for predicting protein backbone torsion angles from NMR chemical shifts. Journal of biomolecular NMR *44*, 213-223.

Sheng, Y., Hong, J.H., Doherty, R., Srikumar, T., Shloush, J., Avvakumov, G.V., Walker, J.R., Xue, S., Neculai, D., Wan, J.W.*, et al.* (2012). A human ubiquitin conjugating enzyme (E2)-HECT E3 ligase structure-function screen. Mol Cell Proteomics *11*, 329-341.

Uzunova, K., Dye, B.T., Schutz, H., Ladurner, R., Petzold, G., Toyoda, Y., Jarvis, M.A., Brown, N.G., Poser, I., Novatchkova, M.*, et al.* (2012). APC15 mediates CDC20 autoubiquitylation by APC/C(MCC) and disassembly of the mitotic checkpoint complex. Nature structural & molecular biology *19*, 1116-1123.

van Heel, M. (1984). Multivariate statistical classification of noisy images (randomly oriented biological macromolecules). Ultramicroscopy *13*, 165–183.

Wickliffe, K.E., Lorenz, S., Wemmer, D.E., Kuriyan, J., and Rape, M. (2011). The mechanism of linkage-specific ubiquitin chain elongation by a single-subunit E2. Cell *144*, 769-781.

Williams, C., van den Berg, M., Panjikar, S., Stanley, W.A., Distel, B., and Wilmanns, M. (2012). Insights into ubiquitin-conjugating enzyme/ co-activator interactions from the structure of the Pex4p:Pex22p complex. The EMBO journal *31*, 391-402.

Wong, L.E., Masse, J.E., Jaravine, V., Orekhov, V., and Pervushin, K. (2008). Automatic assignment of protein backbone resonances by direct spectrum inspection in targeted acquisition of NMR data. J Biomol NMR *42*, 77-86.

Young, T.S., Ahmad, I., Yin, J.A., and Schultz, P.G. (2010). An enhanced system for unnatural amino acid mutagenesis in E. coli. Journal of molecular biology *395*, 361-374.

Zhao, H., Brautigam, C.A., Ghirlando, R., and Schuck, P. (2013a). Overview of current methods in sedimentation velocity and sedimentation equilibrium analytical ultracentrifugation. Current protocols in protein science / editorial board, John E Coligan [et al] *Chapter 20*, Unit20 12.

Zhao, H., Ghirlando, R., Piszczek, G., Curth, U., Brautigam, C.A., and Schuck, P. (2013b). Recorded scan times can limit the accuracy of sedimentation coefficients in analytical ultracentrifugation. Anal Biochem *437*, 104-108.